Journal of Materials Chemistry B

Accepted Manuscript

ROYAL SOCIETY OF CHEMISTRY

www.rsc.org/materialsB

A Series of Zn(II) Terpyridine Complexes with Enhanced Two-Photon-Excited Fluorescence for *in Vitro* and *in Vivo* Bioimaging†

Qiong Zhang,‖[a,b] Xiaohe Tian,‖[c] Zhangjun Hu,‖[b] Caroline Brommesson,[b] Jieying Wu,*[a] Hongping Zhou,[a] Shengli Li,[a] Jiaxiang Yang,[a] Zhaoqi Sun, *[d] Yupeng Tian*[a,e] and Kajsa Uvdal[b]

‖ *These authors contributed equally to this work*

Abstract: There has still been a challenge to obtain two-photon excited fluorescent bioimaging probes with intense emission, high photo-stability and low cytotoxicity. At present work, four Zn(II)-coordinated complexes (**1**-**4**) constructed from two novel D-A and D-π-A ligands ($\mathbf{L_1}$ and $\mathbf{L_2}$) are investigated both experimentally and theoretically, aiming to explore efficient two-photon probes for bioimaging. The molecular geometry optimization used for the theoretical calculations is obtained from the crystallographic data. Notably, the results indicate that the complexes **1** and **2** display enhanced two-photon absorption (2PA) cross sections compared their corresponding D-A ligand ($\mathbf{L_1}$). Furthermore, it was found that the complex **1** exhibits the advantages, including moderate 2PA cross section in the near-infrared region, longer fluorescence lifetime, higher quantum yield, good biocompatibility and enhanced two-photon excited fluorescence. Therefore, complex **1** is evaluated as bioimaging probe for HepG2 cells *in vitro* imaging, in which it is observed under two-photon scanning microscopy that the complex **1** exhibits effective co-staining with endoplasmic reticulum (ER) and nuclear membrane; as well as for zebrafish larva *in vivo* imaging, in which it is observed that the complex **1** exhibits the specificity in the intestinal system.

Introduction

There has been considerable interest in developing organic/inorganic hybrid materials[1-4] with large two-photon absorption (2PA) cross section (σ, expressed in GM = 1×10^{-50}cm^4 s photon^{-1} molecule^{-1}) in recent years, owing to their potential applications in photodynamic therapy[5-6], photochemical delivery of biological messenger[7-9], confocal microscopy[10-13], three dimensional data storage[14-15], micro-fabrication and optical power limiting.[16-17] These applications strongly rely on the large 2PA cross sections of the precisely-engineered organic molecules or complexes. Several features are significant with respect to the 2PA spectra of the compounds specifically, those systems exhibit pronounced 2PA with σ values greater than 500 GM over a broad spectral window, in some cases ranging from 600-900 nm.[18-21] Fluorescent compounds with large 2PA cross sections are significantly important for working as two-photon fluorescent probes, as they have increased penetration depth (greater than 500 μm), localized excitation, prolonged observation time and reducing photo-induced damage. However, apart from the high 2PA cross sections, applicable 2PA materials for bioimaging applications have to satisfy various other basic requirements, such as water solubility and biocompatibility.

[a]*Department of Chemistry, Key Laboratory of Functional Inorganic Materials Chemistry of Anhui Province, Anhui University, Hefei 230039, P. R. China E-mail: yptian@ahu.edu.cn; jywu1957@163.com*
[b] *Division of Molecular Surface Physics & Nanoscience, Department of Physics, Chemistry and Biology (IFM), Linköing University, 58183 Linköing (Sweden)*
[c] *Department of Chemistry, The MRC/UCL Centre for Medical Molecular Virology, University College London, WC1H 0AJ, London, UK*
[d] *School of Physics and Material Science, Anhui University, Hefei 230601, P. R. China E-mail:szq@ahu.edu.cn*
[e] *State Key Laboratory of Coordination Chemistry, Nanjing University, Nanjing 250100, P. R. China*

Over the past decades, the design of fluorescent chromophore targeting either specific intracellular structures or chemical species has progressed rapidly.[22-23] However, conventional molecules with large 2PA cross sections tolerate high molecular weight, extended π-conjugation system, low solubility, significant synthetic work and financial cost-scaling[24-28], which are obstacles to their extensive use for those bio-applications to some extent.

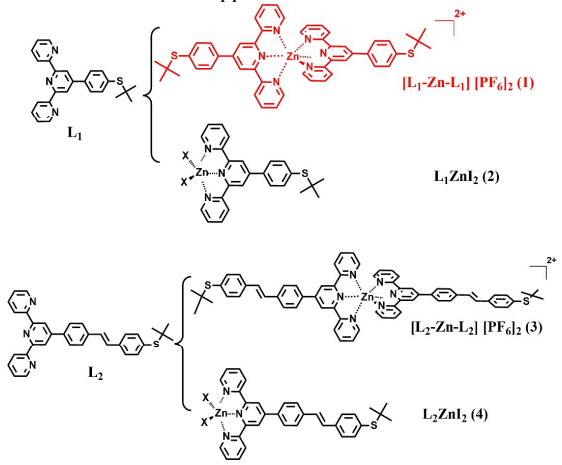

Scheme 1 Molecular structures of the ligands ($\mathbf{L_1}$, $\mathbf{L_2}$) and their metal complexes (**1**-**4**).

Compared to the well-developed studies on the 2PA organic compounds, the research on the 2PA metal-complexes is still an infant stage. Actually, in the recent years, there has been some trying on multi-photon bioimaging by using coordination metal complexes as multi-photon fluorescent probes.[29-32] Metal-complexes can be easily synthesized in high yield by using ligand with low molecular weight, but be conceived to show better physical and chemical properties. This is because that the metal ions can serve either as a multidimensional template for increasing the molecular number density of two-photon active components (i. e. ligands), or as an important structural control over the intramolecular charge transfer process for modulating the σ values.[33-35] The initial investigations on the coordination metal complexes have revealed that the control of the functional organic ligands and the metal ion centre are interconnected, which is of

crucial importance to optimize physical properties of the coordination metal complexes.[36-37] Therefore, developing novel complexes not only with large 2PA cross sections, but also with strong fluorescence, low cytotoxicity, high stability, and low molecular weight, for biomedical applications becomes a challengeable and meaningful work in the field of 2PA materials.

Spurred by this, we designed and synthesized two novel ligands ($\mathbf{L_1}$ and $\mathbf{L_2}$) and their Zn (II) complexes (Scheme 1). The strategy is based on the following considerations: (1) 2, 2': 6', 2"-terpyridine serves as basic multidentate unit, which has electron-withdrawing (A) ability and their structural analogy with rich coordination chemistry have been extensively studied for their high binding affinity towards a variety of metal ions, resulting in interesting photophysical properties;[38-44] (2) tert-butylthiophenyl group works as an intermediate electron-donating (D) group, in which tert-butyl group serves as a steric hindrance to diminish π-π stacking effect, as well as suitable solubility; (3) a styryl unit as an extended π-conjugated system was inserted between terpyridine and tert-butylthiophenyl groups to construct $\mathbf{L_2}$ for comparison with $\mathbf{L_1}$; (4) four complexes were synthesized by selecting closed-shell d^{10}-metals zinc(II). The complexation would be likely to achieve enhanced 2PA properties due to the lack of d-d transitions in comparison with the others.[45-46] And the photophysical properties of all the novel complexes were systematically investigated compared to the their free ligands. Relying on the comprehensive studies of them, Zn (II) complex **1** was selected for bioimging application. Bioimaging study using two-photon scanning microscopy shows that HepG2 cells can be sufficiently stained with **1** specifically and it is capable of specific monitoring the fluorescence signals in the intestinal system of living zebrafish larva at a depth of >100 μm. All these results suggest that **1** is a potential two-photon fluorescent probe for *in vitro* and *in vivo* bioimaging.

Results and Discussion

Structures of the ligand $\mathbf{L_1}$ and $\mathbf{L_2}$ Ligands $\mathbf{L_1}$ and $\mathbf{L_2}$ crystallize in space group $P2_1/c$ and triclinic group $P\bar{1}$, respectively. Figure 1 and S1 show the structures of the molecules with the atomic numbering schemes. For $\mathbf{L_1}$, the dihedral angle between P1 and the phenyl plane P2 was only 24.5°, the linkage between these two planes was conjugated with bond lengths of 1.484(5) (C4–C7), 1.291(4) (C7=C8), and 1.463(5) Å (C8–C9). For $\mathbf{L_2}$, the dihedral angle between P0 and plane P1 was 38.36°, and the linkage between P0 and benzene planes (labeled P1) was conjugated with bond lengths of 1.486 Å (C16–C18), making the covalent bond length (1.486 Å) to be intermediate between normal C-C single bond length 1.54 Å and C=C double bond length 1.38 Å. [47] To sum up, these structural characters suggest that all non-hydrogen atoms between donor and terpyridine acceptor are highly conjugated, being conducive to the charge transfer from sulfide phenyl to the pyridyl unit.

Structures of the complexes

Type I: five-coordinated complexes

The complex **2** crystallizes in the triclinic P$\bar{1}$ space group (supporting Table S1). In the crystal of complex **2**, there are two crystallographic and conformational independent molecules in the asymmetric unit cell, as shown in Figure S1.Within the complex **2**, the metal centre adopts a five-coordinated geometry. Because of the steric demand, the terpyridine ligands coordinate to the Zn (II) centre with a bonding angle for N1-Zn1-N3, which shows deviation from the ideal values of 90° and 180°. The bond lengths of Zn-I in **2** are in the 2.554-2.586 Å range, showing that there is a higher degree of electron delocalization in the Zn-tpy complex.

Type II: six-coordinated complexes

The complex **1** crystallizes in the monoclinic crystal system (supporting Table S1). As shown in Figure 1 and S1, the structure displays the expected geometry with both ligands coordinated in tridentate meridional fashion to the metal centre. As expected, there is no apparent steric hindrance to prevent the free rotation of pyridine and further coordination with metal cations.

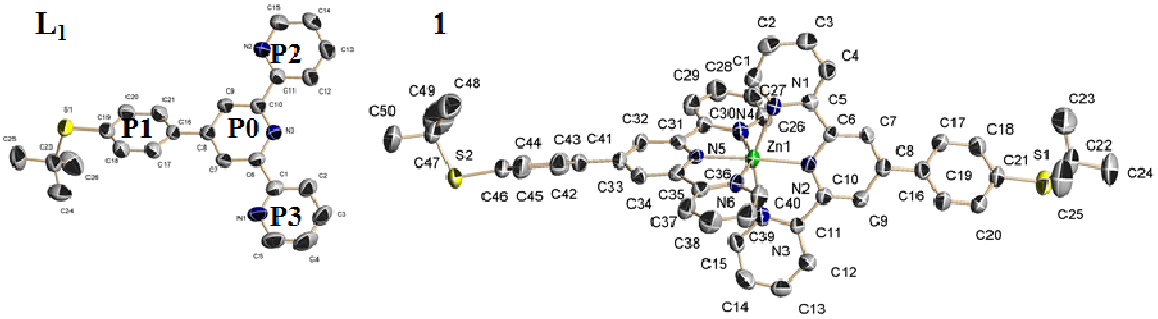

Figure 1 The molecular structures of $\mathbf{L_1}$ and **1** (H atoms and PF_6 ions were omitted for clarity).

The metal-nitrogen bond lengths in **1** are within 2.062-2.397Å range, whereas in related references they are in the range of 1.997-2.234 Å.[48] Otherwise, the equatorial coordination sphere containing Zn and three N atoms in the complex **1** greatly extends electronic delocalization rather than that of **2**, thus benefiting the excited-state charge redistribution and enhancement of 2PA response.

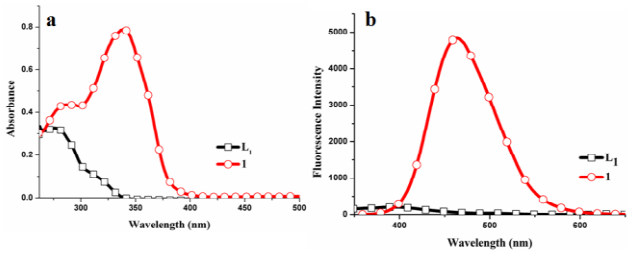

Figure 2 (a) OPA spectra of $\mathbf{L_1}$ and **1** ($c = 1.0 \times 10^{-5}$ mol L^{-1}) in DMF (b) OPEF spectra of $\mathbf{L_1}$ and **1** in DMF

Photophysical Properties

The linear absorption and fluorescence properties for all the compounds in the different solvents were investigated, which were summarized in Table S3.

Linear absorption and computation details The UV-vis absorption spectral data of the both two ligands $\mathbf{L_1}$ and its relevant complex **1** in DMF are given in Figure 2. As shown in Figure 2a, $\mathbf{L_1}$ mainly presents a broad absorption band around 276 nm and a shoulder around 315 nm in absorption spectra. The TD-DFT {[6-31G(d)]} calculations (Figure 3 and Table 1) indicate that the high energy transition presents marked charge transfer (CT) character, with the HOMO and the LUMO being mainly located on the 4 - (tert - butylthio) phenyl unit (denoted as π_D) and S–phenyl unit (denoted as $\pi^*_{S-phenyl}$) with moderate contribution from terpyridine unit (denoted as π^*_A), respectively. The remaining one band (λ_{max} = 289.4 nm, f = 0.76) is assigned mainly to a $\pi_D \rightarrow \pi^*_A$ transition as a result of the HOMO–1→LUMO+1 transition with some contributions from an ICT transition [$\pi_D \rightarrow \pi^*_{S-phenyl}$, HOMO-2→ LUMO]. The lowest energy excitation band of $\mathbf{L_1}$ at 323.8 nm (f = 0.16) is assigned as the intramolecular charge transfer (ICT) transition [$\pi_D \rightarrow \pi^*_{S-phenyl\ \&}\ \pi^*_A$] because of the HOMO-1→LUMO transition (Table 1). Complex **1** shows a weak positive solvatochromic (4−16 nm) absorption behavior, as a result of no significant permanent ground-state dipole moment in polar solvents.[49] For **1**, the most intense transitions (339.0 nm) (Figure 2a) was contributed by the excitation involving several molecular orbitals, with a predominant weight of excitations from HOMO-1→LUMO with the HOMO-1 and the LUMO being mainly located on sulfur atom π character and π* orbitals of terpyridine unit with minor Zn dyz, respectively (Figure 3). These transitions are in keeping with the calculation results (337.4 nm, Table 1), which are contributed to two classes of transitions. One corresponds mainly to CT transition from the sulfide group to the terpyridine part and zinc centre, the complex **1** can arise from a locally excited (LE) transition as single-electronic transition localized in the D-A system.[52] Furthermore, it is accompanied by a 4-5 fold escalation of the extinction coefficient of low energy transition.

One-Photon Excited Fluorescence (OPEF) Properties

The fluorescence properties of all the compounds and complexes in five different solvents are investigated and listed in Table S3, including fluorescence quantum yields and lifetimes (corresponding figures S3-S8 are given in the Supporting Information as well).

Except for the differences on the linear absorption, the enhanced one-photon excited fluorescence of complex **1** compared with $\mathbf{L_1}$ were also observed (Figure 2b). No similar trends of fluorescence changes, however, were found for their corresponding D-π-A systems of complex **3** compared with $\mathbf{L_2}$ (Figure S9). It may be inferred that the directly conjugated terpyridine system and the closed-shell d^{10}-metal centres (Zn) are both responsible for the thus enhanced fluorescence.[50] The largely enhanced fluorescence was only observed for complex **1** against $\mathbf{L_1}$. It can be concluded that such coordination between Zn (II) and $\mathbf{L_1}$ could be enable the fluorescence enhancement of d^{10}-metal complexes,[51] and the possibility that the heavy atom (Iodine) consumes energy from the excited state molecule could be applied to interpret that **2** only shows very modest fluorescence enhancement against $\mathbf{L_1}$. The dual emission of $\mathbf{L_1}$ (Figure S3)apparently arises from the twisted structure of the D-A configuration, while dual-emission were not seen for either complex **1** or **2**, which further suggests that the characteristic dual-fluorescence feature is from a twisted intramolecular charge transfer (TICT) transition.[52-53]

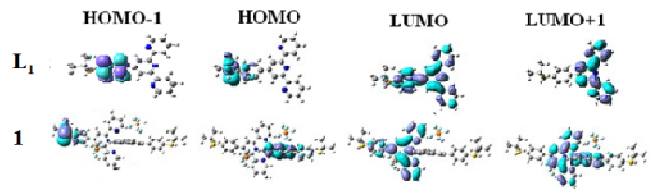

Figure 3 Molecular orbital diagram for $\mathbf{L_1}$ (B3LYP/6-31G(d)) and **1** (B3LYP/LANL2DZ) (the two colors of electron clouds is representative of the square of the wave function of atomic orbitals).

Singlet-state lifetime The fluorescence lifetimes (τ) of the complexes **1-4** are a little longer than those of the ligand $\mathbf{L_1}$ and $\mathbf{L_2}$ when they are all under the excitation wavelength of 360 nm (supporting Table S3). The short singlet-state lifetime in the complexes is consistent with inter-system crossing being very rapid because of the strong spin-orbital coupling induced by mixing of the ligand (π and π^*) and metal dπ orbitals.

Fluorescence quantum yield The fluorescence quantum yields (Φ) of all the compounds in different solvents are determined using coumarin as a standard. The quantum yields of the ethylenic conjugated system in each compound show the sequence of $\mathbf{L_2}$ (0.70) > **4** (0.48) > **3** (0.32) in DMF, while another system follows the order of **1** (0.34) > $\mathbf{L_1}$ (0.16) > **2** (0.04). Since the fluorescence quantum yield process is affiliated with an energetically unstable state, it can be sensitive to a great variety of internal factors defined by the chromophore's structure and external surrounding factors including polarity. Obviously, in DMF, **2** shows much lower quantum yields compared to those of

the other complexes, the results can mainly be explained by the photo-isomerization, *viz,* the molecular planarity is reduced due to the rotating of the flexible-center when the molecules accept energy in the dilute solution.

Lippert-Mataga plot

The magnitudes of dipole moment change (μ_e-μ_g) are proportional to the one photon oscillator strengths, so their values can be calculated from the linear absorption spectrum**.**However, (μ_e-μ_g) is rarely determined experimentally, so the design of efficient 2PA compounds has proceeded empirically, with guidance from theoretical calculations of transition moments. As seen in Table S3, the fluorescence spectra showed moderate Stokes shifts depending on the solvent polarity. Further, the solvatochromism is observed, suggesting a large change in dipole moment between ground and excited states. The Lippert-Mataga equation is the most widely used to evaluate the dipole moment changes of the dyes with photoexcitation: [54-55]

$$\Delta\upsilon = \frac{2\Delta f}{4\pi\varepsilon 0hca^3}(\mu e - \mu g)^2 + b \quad (1)$$

$$\Delta f = \frac{\varepsilon - 1}{2\varepsilon + 1} - \frac{n^2 - 1}{2n^2 + 1} \quad (2)$$

in which $\Delta v = v_{abs} - v_{em}$ stands for Stokes shift, v_{abs} and v_{em} are absorption and emission (cm^{-1}), h is the Planck's constant, c is the velocity of light in a vacuum, a is the Onsager radius and b is a constant. Δf is the orientation polarizability, μ_e and μ_g are the dipole moments of the emissive and ground states, respectively, and ε_0 is the permittivity of the vacuum. $(\mu_e-\mu_g)^2$ is proportional to the slope of the Lippert -Mataga plot.

Plots of the Stokes shifts as a function of the solvent polarity factor Δf are shown in Figure S10. Only the data involving the aprotic solvents are shown because application of this analysis with solvents where specific solute-solvent interactions are present is not appropriate. The slope of the best-fit line is related to the dipole moment change between the ground and excited states (μ_e-μ_g). As shown in Figure S10, the slopes of **L_1** and **1**, **2** are -19563, -7198 and -8718, respectively. So the values of μ_e-μ_g were calculated as 3.22 D for **L_1**, 4.35D for **1**, 3.29 D for **2**, respectively (eq 1). The μ_e-μ_g values of the complexes indicate that the molecule in the excited state has an extremely polar structure,[56] an enhanced 2PA response of the complexes was found compared with **L_1**, which is proved by the crystal structures (**L_1**, **1** and **2**) and in good agreement with their nonlinear optical properties as shown in Figure. 4.

Among the occupied states of **1** based on Zn orbitals, the calculated results exhibit that HOMO-1 is comprised of sulfur atom π character while the HOMO is localized in one of the terpyridine units with a small contribution from Zn d_{xz}. Also LUMO distribution is localized in the π* orbitals of the other terpyridine unit with minor Zn d_{yz}. Therefore, there are relatively strong electron interactions between the ligand molecules and the zinc centre, and the electron density in each atom of the ligand is very similar, it can be inferred that there are more electron density on average at the metal ion centre in the charge transfer (CT) state.[57]

Two-Photon Excited Fluorescence (2PEF) Spectroscopy and Two-Photon Absorption (2PA) Cross-Sections

As shown in Figures S3 to S8, there is no linear absorption in the wavelength range 680-900 nm for all the compounds in DMF, which indicates that there is no energy level corresponding to an electron transition in this spectral range. If frequency upconverted fluorescence appears upon excitation with a tunable laser in this range, it should be safely attributed to multiphoton excited fluorescence (Figure S11). Detailed experiments revealed that the peak positions of the 2PEF spectra of these cpmpounds are independent of the excitation wavelengths, but the emission intensities of the 2PEF are dependent on the excitation wavelengths. The electrons can be pumped to the different excited states by 2PA due to the different selection rule; however, they would finally relax to the same lowest excited state *via* internal conversion and/or vibrational relaxation.

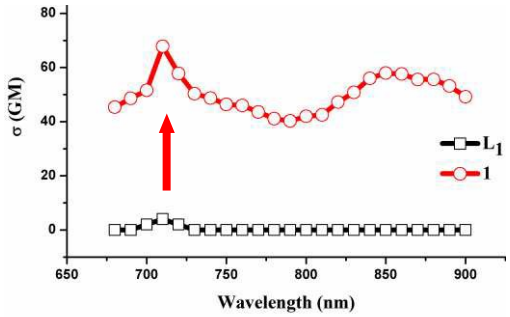

Figure 4 2PA spectra of **L_1** and related complex **1**

The 2PA cross sections (σ) of all compounds were obtained by a comparison of the 2PEF spectra of individual compound with fluorescein in a calibration standard.[58] By tuning the pump wavelengths incrementally from 680 to 900 nm, keeping the input power fixed, almost no 2PEF signal of ligand **L_1** was detected. The 2PEF intensities of complexes **1** and **2** are much increased compared to those of their free ligands **L_1** (supporting Figure S12a**)**.

Two-photon absorption cross-section values σ of the **L_2** ligand have been shown in Figure S13b. The value at 720 nm (139×10^{-50} cm^4 s $photon^{-1}$, 139 GM) can be compared to the values of the other two complexes (around 95-128 GM) at 710 nm. This comparison depends on the wavelength. It was found that almost no increase of the 2PA cross-sections was observed on going from the ligand to its complexes. Such trend is unexpected since it is commonly known that the increase of the conjugation length leads to an increase of the 2PA activity. Since coordination to Zn (II) centre leads to increased acceptor properties of the terpyridine rings of push-pull dipolar ligands, it reasonably modifies the charge transfer form affecting the ground electronic state, as a result of the ligands bonded to the metal ion to form an large extended π-conjugated system in the coordination compound molecules, preventing electron flowing within the whole molecule, in agreement with the observed decrease of the 2PA cross-sections[59-60].

However, it is interesting to point out that the efficiency of push-pull dipolar (D-A) systems has been described by large increasing tendency. As shown, in the measured region, the 2PA

cross-section σ values of complex **1** were significantly enhanced compared to their free ligand $\mathbf{L_1}$ in high polarity solvent DMF. Importantly, the peak 2PA cross-sections appear in the near-infrared range. This large 2PA response comes from the marked core to periphery charge redistribution in complexes upon photoexcitation.[61] Therefore, complexation with Zn (II) enhances the electron-acceptor character of terpyridine group, which converts the ligand to a more strongly polarized D-A unit, which may favor the ICT, causing an enhanced two-photon absorption. The enhanced trend observed in the experiments was consistent with above structural investigation and theoretical calculations (Figure 1, S2 and Table 2). The observed 2PA band is moderately strong: σ = 65 GM in **1** and even stronger (99 GM) in **2**. This should imply a nonrealistically large change of permanent dipole moment because of nonsymmetrical vibration.[62] Significantly, by comparing those with its free $\mathbf{L_1}$, **1** bears moderate active σ value, as well as it exhibits higher quantum yield, longer lifetime in ethanol (supporting Table S3), and smaller molecular volume, which stimulated us further to explore its potential application in biological imaging.

Table 1 Ab initio calculation data of linear absorption spectra, the experimental data of linear absorption spectra, and oscillator strengths of all the compounds in DMSO

	$\mathbf{L_1}$	$\mathbf{L_2}$	**1**	**2**
$\lambda_{ab\text{-}OPA}$ (nm) (calculated) [a]	289.4 323.8	368.4 302.1	337.4	335.7
$\lambda_{ab\text{-}OPA}$ (nm) (experiment, DMF)	276.0 315.0	335.0 282.0	339.0 283.0	321.0 281.0
f [b]	0.76 0.16	1.68 0.24	0.32	0.65
OI and Tc[c]	103 (H-2)→106 (L) (0.42) 104 (H-1)→107 (L+1) (0.54) 104 (H-1)→106 (L) (0.58)	132(H)→133(L) (0.55) 132(H)→135(L+2) (0.62) 131(H-1)→134(L+1) (0.19)	284(H-1)→286(L) (0.60)	115(H-3)→ 123 (L+3)(0.598)

[a] The TD-DFT calculation data of one-photon absorption (OPA) spectra with the peak position of the maximum absorption band (nm), [b] Oscillator Strengths (f) [c] The excited states computed by TDDFT Method with the Orbitals Involved (OI) in the Excitations Including Transition Coefficients (Tc)

Biological Imaging Application of 1

In order to evaluate their application in intracellular imaging, Zn (II) complex **1** was selected due to stronger fluorescence intensity in DMSO/H_2O, higher quantum yield, moderate 2PA cross-section and longer fluorescent lifetime (Table S3). We have conducted cytotoxicity assays in HepG2 cells. Figure S14 shows the cell viability data for HepG2 cells treated with **1** as quantified by the MTT assay, an established method of probing cell death. These data show that HepG2 cells show near 100% viability following 24 h of treatment with 20 μM **1**. Higher concentrations result in decreased cell survival, with 65% and 85% viability observed following 24 h of treatment with 40 μM $\mathbf{L_1}$ and **1**. These cytotoxicity tests show that sub- and low-micromolar concentrations of **1** are low toxic over a period of at least 24 h and could be safely used for further biological studies. Micrographs of one-photon confocal microscopy and two-photon microscopy of HepG2 cells labeled with **1** were captured. **1** was first dissolved in DMSO to 2 mM and then diluted by PBS (phosphate buffer solution) to 40 μM as working concentration. HepG2 cells firstly incubated with 40 μM **1** for 30 minutes and imaged directly without fixation. The live HepG2 cells images (Figure 5a, 63× magnification) exhibited effective cellular uptake (Figure 5a) within the short incubation period. It also showed remarkable stability of intracellular fluorescence as we switch from one-photon excitation (Figure 5b) to two-photon excitation (Figure 5d). It is interesting to note that although **1** indicated similar cellular distribution pattern under one-photon and two-photon excitation, TP excited cells (Figure 5c) showed much less background noise and resulting in an auto-fluorescence free micrograph compare to OP (Figure 5e) excited cells.

A co-staining experiment with Mitotracker® (Figure 5f and g) was performed to further determine that whether **1** was internalized with membrane-rich organelles mitochondria. The merged micrographs (Figure 5a) clearly indicated overlapping either with OP or TP excited channel. It was not unexpected that such complex could effectively uptake by cells due to its small molecular weight, and its relatively good hydrophilic nature and positive charge would imply the uptake mechanism is likely to be endocytosis. Therefore, the above results suggested that **1** was not co-localized with intracellular mitochondria and might stained with other endocytotic compartments.

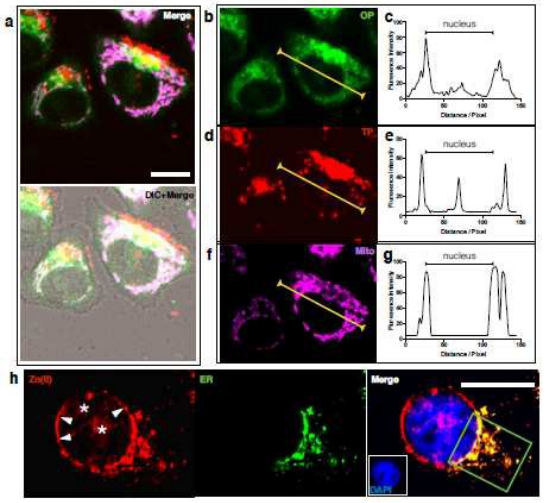

Figure 5 (a) Merged and DIC merged image of HepG2 cells incubated with 40 μM **1** after 30 min of incubation, washed by PBS buffer. (b) One-photon image of HepG2 cells incubated with 40 μM **1** after 30 min of incubation, washed by PBS buffer. λ_{ex} = 405 nm

(emission wavelength from 440 to 480 nm). (c, e, g) Fluorecense intensity profile of complex **1** cross a single cells corr esponding to the line segment from b, d and f. (d) Two-photon image of HepG2 cells incubated with 40 μM **1** after 30 min of incubation, washed by PBS buffer. λ_{ex} = 700 nm (emission wavelength from 543 to 606 nm). (f) One-photon image of HepG2 cells incubated with Mitotracker. λ_{ex} = 633 nm (emission wavelength from 650 to 700 nm). (h) Two-photon image of HepG2 cells incubated with 40 μM **1,** λ_{ex} = 700 nm (emission wavelength from 543 to 606 nm) and One-photon image of HepG2 cells incubated with ER tracker, λ_{ex} = 488 nm (emission wavelength from 500 to 550 nm) .

.

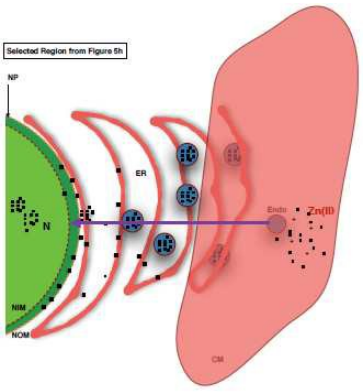

Figure 6 Schematic representation of Zn (II) complex crossing the cell membrane via endocytosis and penetrating into ER and cell nucleaus (Endo: Endosome, CM: cell membrane, ER: endoplasmic reticulum. N: nucleus, NP: nuclear pores, NIM: nuclear inner-membrane, NOM: nuclear outer-membrane).

Therefore we then captured a higher resolution live-cell micrograph (100×) stained with **1** under TP excitation and co-stained with ER tracker and DAPI. Figure 5h showed much more intracellular details under TP confocal microscopy and clearly indicated nice (red merge green make yellow) co-localization between endoplasmic reticulum (ER) and **1** at certain region. It was not surprised; as ER closely associated with cell membrane, endosomal system and cell nucleus, play a crucial role in endosomal cargo sorting and protein synthesis. It is noteworthy that **1** staining with other endomembrane system including nuclear membrane (Figure 5h, arrows) and even nuclear region (Figure 5h, stars) also observed. Since nuclear region lack of endosomal/lysosomal compartment, this might suggest the free release of **1** from endocytotic pathway from ER and uniformly distributed on the dynamic nuclear membrane, and consequently the positively charger Zn (II) complex partially penetrated into negatively charged cell nuclear (Figure 6) DNA. In addition, cytotoxicity is a potential side effect of **1** that must be controlled when dealing with living cells or tissues.

Besides the imaging ability in living cells of **1**, the first ratiometric in *vivo* imaging in 3-dayold zebrafish larva was also investigated *via* staining the larva by **1** (30 μM, 4 h). As shown in Figure 7a, the OPM images of the larva head exhibit mainly two regions of bright fluorescence. The 2PM image obtained from band paths 543-606 nm displays the red regions on the same location, indicating the higher **1** level in these two bright spots than that in the rest of field. Only very minor green and red spots

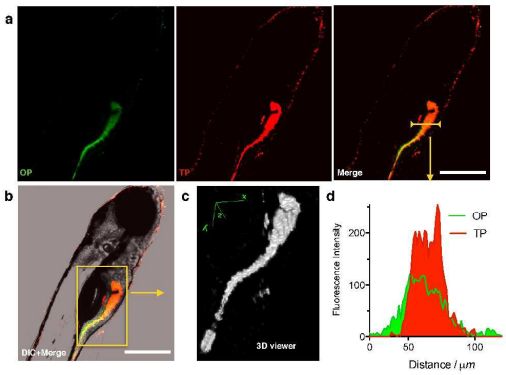

Figure 7 (a) One-photon image of 72 h-zebrafish larva incubated with 30 μM **1** after 4 h of incubation, washed by PBS buffer. λ_{ex} = 405 nm (emission wavelength from 440 to 480 nm); Two-photon image of 72 h-zebrafish larva incubated with 30 μM **1** after 4 h of incubation, washed by PBS buffer. λ_{ex} = 700 nm (emission wavelength from 543 to 606 nm); The overlay of 1PA and 2PA images. (b) The overlay of bright field and (a). (c) Two-photon excited fluorescence 3D images of zebrafish larva reconstructed from selected region from (b) (d) One and two photon fluorescence intensity of 72 h-zebrafish larva incubated with 30 μM **1**, from selected segment from (a). The scale bars represent 100μm.

can be found in peripheral areas in ratiometric image. The overlay of TP, OP and bright-field images discloses one of the bright regions located in the intestinal system (Figure 7b). Moreover, the TP signal again showed much less background noise, higher intensity and more specified staining within intestinal system (Figure 7d). Comparison between the ratiometric images of $\mathbf{L_1}$ treated zebrafish larva and the **1** treated larva suggests that zebrafish incubated with control ligand $\mathbf{L_1}$ indicated expected intestinal system localization (Supporting Information, Figure S15). Both one- and two-photon fluorescence microscopies provided similar imaging results to **1.** However, the fluorescence intensity of $\mathbf{L_1}$ is significantly weaker than **1** (compare with Figure 7). The 2PM images revealed that **1** distributed in intestinal region at 128.2 μm depth (Figure 7c). Control experiments were carried out with zebrafish larva treated with $\mathbf{L_1}$, which was shown to detect fluorescence signals of the tissues only at a depth of up to 55 μm (Figure S15). This much deeper penetration, coupled with the significantly lower background fluorescence and better clarity observed in the 2PM images, clearly demonstrated the potential application of these newly developed, two-photon probes for tissue-based imaging experiments in future.

To further prove the stability of the complex **1**, the variable temperature ^{1}H NMR of **1** has been measured (supporting Figures S16). The result indicates that the well resolved peaks of the spectra exhibit almost no change in the temperature range of 273~303K, which proves that the solid structure of $[\mathbf{L_1}Zn\mathbf{L_1}]^{2+}$cation is still kept in solution. Additionally, their crystal structures were further confirmed by single crystal X-ray diffraction analysis. The unusual two-photon luminescent properties and the low cytotoxicity of **1** make it a potential candidate as novel luminescence material for live cell imaging.

Conclusions

Four novel Zn (II) complexes with $\mathbf{L_1}$ and $\mathbf{L_2}$ as ligands have been synthesized and determined. The results showed that the complexes based on two types of terpyridine ligands (D-π-A and

D-A) can arouse different optical properties. It was notable that more intensive OPEF and 2PEF, and significant increased two-photon cross section values were obtained for the Zn(II) complexes compared to those of their free ligand $\mathbf{L_1}$. It was proposed that the increased fluorescence could be contributed by closed-shell d^{10} feature of Zn(II). And an extended conjugated bridge, facilitating the π-electron contribution from the metal ions in the $\mathbf{L_1}$ system within the complexes, may favor the ICT, thus causing enhanced two-photon absorption. As was expected, the complex **1** was successfully applied as 2PA probe for *in vivo* and *in vivo* bioimaging. ER and nuclear membrane staining in live cells and the uptake mechanism were discussed in detail. Furthermore, complex **1** has been utilized to visualize the intestinal system of live zebrafish larva *in vivo* . The results favor that **1** may be a potential biocompatible and long-term *in vivo* imaging agent.

Experimental Section

Preparation of 4'-(4-(tert-butylthio)phenyl)-2,2':6',2''-terpyridine ($\mathbf{L_1}$): *t*-BuOK (1.6 g, 13.9 mmol) was dissolved in 30 mL THF, and 2-aceylpyridine (1.1 g, 8.95 mmol) was added to the solution. After the reaction mixture was stirred at room temperature for 2 h, a (0.73g, 4 mmol) was added dropwise. After the reaction mixture was stirred at room temperature for 8 h, the ropy mixture was added to a stirred solution of ammonium acetate (12.0 g, excess) in ethanol (250 mL). The reaction was heated at reflux for 5 h, affording a dark red solution. Cooled to the room temperature, bright yellow product was crystallized from the filtered solution. The yellow granular product was recrystallized from ethanol and dried in vacuum to give T with yield 68%. ^{1}H NMR (DMSO-d_6, 400 MHz): (ppm) = 1.31 (s, J = 9H), 7.53-7.56 (t, J = 6.00 Hz, 2H), 7.69-7.71 (d, J = 8.00 Hz, 2H), 7.94-7.96 (d, J=8.00, 2H), 8.03-8.07 (t, J = 7.60 Hz, 2H), 8.68-8.69 (d, J = 4.0 Hz, 2H), 8.73 (s, 2H), 8.77-8.78 (d, J = 4.00 Hz, 2H); ^{13}C NMR (DMSO-d_6, 100 MHz): (ppm) = 155.72, 154.79, 149.33, 148.65, 137.79, 137.62, 137.51, 133.73, 127.22, 124.60, 120.94, 117.94, 46.18, 30.70; FT-IR (KBr, cm^{-1}): v = 2958 (s), 2921 (w), 1796 (w), 1747 (w), 1735 (w), 1717 (w), 1700 (w), 1685 (w), 1672 (m), 1651 (s), 1583 (s), 1540 (s), 1510 (w), 1492(w), 1470 (s), 1440 (m), 1403 (w), 1384 (s), 1364 (m), 1265 (m), 1167 (s), 1142 (w), 1090 (w), 1073 (m), 1037 (w), 1017 (w), 993 (w), 891 (w) 834 (m), 790 (s), 734 (s), 661 (m), 641 (m), 620 (m), 580 (w), 528 (w). $C_{25}H_{23}N_3S$: Calcd. C 75.53, H 5.83, N 10.57. Found: C 75.68, H 5.81, N 10.60. HRMS (GCT-MS) calcd for $C_{25}H_{23}N_3S$: 397.54; Found, 398.09.

Preparation of (E) - 4' - (4 - (4 - (tert - butylthio) styryl) phenyl) - 2, 2' : 6', 2'' - terpyridine ($\mathbf{L_2}$): 4-(2, 2': 6', 2''-Terpyridyl-4')-benzyltriphenylphosphonium bromide[46] (2.0 g, 3.0 mmol), 4-Formyl-S-tert-butylphene (0.55 g, 3.0 mmol) and *t*-BuOK (1.3 g, 12.3 mmol) were placed into a dry mortar and milled vigorously for about 20 mins, and monitored by TLC until reaction completion. The mixture was dispersed in 100 mL ethanol. The residual solid was filtered and recrystallized from water/ethanol, giving pale yellow crystals of L with yield 77%.^{1}H NMR (DMSO-d_6, 400 MHz): (ppm) =1.27 (s, 9H), 7.30-7.32 (d, J = 8 Hz, 1H), 7.42 (s, 3H), 7.51-7.54 (t, J = 6.00 Hz, 3H), 7.67-7.87 (d, J = 8.00 Hz, 1H), 7.83-7.84 (d, J = 4.00 Hz, 2H), 7.96-7.98 (d, J = 8.00 Hz, 2H), 8.04-8.05 (d, J = 4.00 Hz, 2H), 8.68-8.70 (d, J = 8.00 Hz, 3H), 8.75-8.78 (t, J = 12.00 Hz, 3H); ^{13}C NMR (DMSO-d_6, 100 MHz): (ppm) = 155.68, 154.93, 149.31, 137.45, 131.51, 130.26, 130.13, 129.98, 129.52, 128.83, 127.55, 127.25, 126.85, 124.52, 120.94, 117.61, 45.96, 30.65; FT-IR (KBr, cm^{-1}): v = 2956 (w), 2919 (w), 1717 (w), 1701 (w), 1685 (w), 1651 (w), 1602 (s), 1581 (s), 1564 (s), 1541 (m), 1511 (m), 1467 (s), 1440 (m), 1416 (m), 1389 (s), 1361 (m), 1263 (m), 1094 (s), 1037 (m) 989 (m), 964 (s), 947 (w), 876 (w), 834 (s), 792 (s), 736 (s), 678 (m), 659 (m), 620 (m), 577 (w) 541 (s) 508 (w). $C_{50}H_{46}ZnF_{12}N_6P_2S_2$: Calcd. C 52.20, H 4.03, N 7.31. Found: C 52.18, H 4.05, N 7.29. HRMS (GCT-MS), $C_{50}H_{46}ZnN_6S_2$: 858.25, *found:* 860.0 [M+H, 100%].

Preparation of $[\mathbf{L_1}\text{-Zn-}\mathbf{L_1}]$ $[PF_6]_2$ (1): Complex **1** was prepared by a procedure similar to that for **3.** 0.044 g (0.2 mmol) in place of $Zn(OAc)_2{\cdot}2H_2O$. ^{1}H NMR (DMSO-d_6, 400 MHz): (ppm) =9.44 (s, 2H), 9.18-9.20 (d, J=4.00, 3H), 8.52-8.53 (d, J=4.00, 3H), 8.31 (s, 3H), 7.99-8.03 (t, J=8.00, 6H), 7.73-7.75 (d, J=8.00, 3H), 7.52-7.58 (m, 8H), 1.30 (s, 18H); ^{13}C NMR (DMSO-d_6, 100 MHz): (ppm) = 154.36, 149.45, 147.80, 141.27, 139.81, 137.29, 134.34, 129.84, 128.60, 127.52, 123.53, 120.62, 46.05, 30.68; FT-IR (KBr, cm^{-1}): v = 1796 (m), 1735 (w), 1600 (s), 1573 (s), 1544 (s), 1477 (w), 1421 (m), 1363 (m), 1248 (m), 1017 (s), 974 (m), 832 (s), 791 (m), 732 (m), 682 (m), 659 (m), 638 (m), 557 (s), 542 (m). $C_{50}H_{46}ZnF_{12}N_6P_2S_2$: Calcd. C 52.20, H 4.03, N 7.31. Found: C 52.18, H 4.05, N 7.29. HRMS (GCT-MS), $C_{50}H_{46}ZnN_6S_2$: 858.25, *found:* 860.0 [M+H, 100%].

Preparation of $\mathbf{L_1}ZnI_2$ (2): Complex **2** was prepared by a procedure similar to that for **1**. ^{1}H NMR (DMSO-d_6, 400 MHz) (ppm) = 9.43 (s, 1H), 9.16-9.19 (d, J=12.00, 2H), 9.06-9.07 (d, J=8.00 1H), 8.96 (s, 1H), 8.33-8.45 (d, J = 8.00 Hz, 2H), 8.30 (s, 2H), 7.95-7.96 (d, J=4.00 2H), 7.86-7.87 (d, J=4.00, 1H), 7.78-7.80 (d, J=8.00, 1H), 7.50-7.52 (t, J=4.00, 1H), 1.38 (s, 9H).^{13}C NMR (DMSO-d_6, 100 MHz): (ppm) = 156.43, 155.11, 148.65, 146.41, 141.18, 137.34, 137.28, 128.38, 127.68, 123.43, 121.27, 120.63, 46.47, 30.76; FT-IR (KBr, cm^{-1}): v = 2958 (w), 2922 (w), 1786 (w), 1773 (w), 1747 (w), 1735 (w), 1717 (w), 1700 (w), 1685 (w), 1651 (w), 1612 (s), 1573 (m), 1560 (m), 1541 (s), 1523 (w), 1509 (w), 1474 (s), 1459 (m), 1423 (m), 1393 (m), 1363 (w), 1340 (w), 1297 (w), 1249 (w), 1161 (m), 1096 (w), 1067 (w), 1013 (s), 895 (w), 829 (m), 792 (s) 732 (w), 677 (w), 658 (w), 637 (w), 531 (w). $C_{25}H_{23}I_2ZnN_3S$: Calcd. C 41.89, H 3.23, N 5.50. Found: C 42.01, H 3.24, N 5.48. HRMS (GCT-MS), $C_{25}H_{23}I_2ZnN_3S$: 714.90, *found:* 587.13 [M-I, 100%].

Preparation of $[\mathbf{L_2}\text{-Zn-}\mathbf{L_2}]$ $[PF_6]_2$ (3): $\mathbf{L_2}$ (0.200g, 0.4 mmol) and $Zn(OAc)_2{\cdot}2H_2O$ 0.053 g (0.2 mmol) were dissolved in MeOH (10 mL). The mixture was refluxed for 2 h at 70 °C and then 10mL MeOH containing NH_4PF_6 0.065 g (0.4 mmol) was added in. The mixture stirred for 30 min to give a clear yellow solution. Yellow crystals suitable for X-ray diffraction analysis were obtained after two weeks by slow evaporation of the methanol solution at room temperature. ^{1}H NMR (DMSO-d_6, 400 MHz): (ppm) =9.44 (s, 4H), 9.18-9.20 (d, J=8.00, 4H), 8.52-8.54 (d, J=8.00, 4H), 8.29-8.33 (t, J=8.00, 4H), 7.98-8.04 (m, 8H), 7.73-7.51 (d, J=8.00, 4H), 7.51-7.59 (m, 2H), 1.30 (s, 18H). ^{13}C NMR (DMSO-d_6, 100 MHz): (ppm) = 154.38, 149.46, 147.74, 141.28, 139.63, 137.37, 137.30,

136.98, 134.35, 131.88, 129.86, 128.87, 128.60, 128.57, 127.67, 127.53, 126.98, 46.05, 30.68; FT-IR (KBr, cm^{-1}): ν = 2957 (w), 2920 (w), 1796 (m), 1700 (w), 1651 (w), 1579 (s), 1572 (m), 1541 (m), 1475 (s), 1521 (w), 1459 (m), 1400 (m), 1424 (m), 1361 (m), 1247 (m), 1161 (s), 1096 (w), 1012 (s), 967 (m), 874 (m), 836 (m), 788 (s),681 (m), 540 (s). $C_{66}H_{58}ZnF_{12}N_6P_2S_2$: Calcd. C 58.52, H 4.32, N 6.20. Found: C 58.34, H 4.33, N 6.22. HRMS (GCT-MS), $C_{66}H_{58}ZnN_6S_2$: 1062.35, *found:* 1062.10 [M, 100%].

Preparation of L_2ZnI_2 (4): L_2 (0.200g, 0.4 mmol) was dissolved in 5 mL CH_2Cl_2 and adding 10 mL MeOH containing $ZnI_2 \cdot 2H_2O$ (0.141 g, 0.4 mmol) with refluxing at 70°C for 2h. Cooled to the room temperature, bright yellow product was crystallized from the filtered solution. Yellow crystals suitable for X-ray diffraction analysis were obtained after two weeks by slow evaporation of the methanol solution at room temperature. ^{1}H NMR (DMSO-d_6, 400 MHz): (ppm) = 1.30 (s, 9H), 7.43-7.46 (d, *J*=12.00, 1H), 7.48-7.56 (m, 3H), 7.65-7.68 (d, *J*=12.00, 2H), 7.88-7.99 (m, 4H), 8.19 (s, 1H), 8.26-8.40 (m, 3H), 8.48-8.50 (d, *J*=8.00, 1H), 8.99-9.00 (d, *J*=4.00, 1H), 9.05-9.07 (d, *J*=8.00, 1H), 9.17 (s, 1H), 9.20-9.22 (d, *J*=8.0, 1H), 9.39-9.43 (d, *J*=16.00, 1H); ^{13}C NMR (DMSO-d_6, 100 MHz): (ppm) = 148.47, 148.29, 147.04, 141.16, 140.87, 137.22, 131.96, 131.90, 131.66, 129.58, 128.35, 128.31, 127.23, 126.71, 123.08, 120.69, 119.98, 45.86, 30.66; FT-IR (KBr, cm^{-1}): ν = 2962 (w), 1796 (w), 1772 (w), 1734 (w), 1716 (w), 1699 (w), 1650 (m), 1598 (s), 1613 (s), 1573 (m), 1542 (m), 1521 (m), 1474 (s), 1425 (m), 1402 (s), 1363 (m), 1248 (m), 1160 (m), 1067 (w), 1013 (m), 968 (m), 874 (m), 836 (m), 789 (s), 729 (m), 682 (m), 636 (m), 541 (m). $C_{33}H_{29}I_2ZnN_3S$: Calcd. C 48.40, H 4.32, N 5.13. Found: C 48.32, H 4.37, N 5.14. HRMS (GCT-MS), $C_{33}H_{29}I_2ZnN_3S$: 816.95, *found:* 817.11 [M+H, 100%].

Acknowledgment This work was supported by grants from the National Natural Science Foundation of China (51372003, 21271004, 51272001, 51472003, 51432001 and 21271003), Ministry of Education Funded Projects Focus on returned overseas scholar, Program for New Century Excellent Talents in University (China) and Doctoral Program Foundation of Ministry of Education of China (20113401110004), China Postdoctoral Science Foundation (2015M571912), the Swedish Research Council (VR) (621-2013-5357) and Swedish Government strategic faculty grant in material science (SFO, MATLIU) in Advanced Functional Materials (AFM).

Supporting Information Available: †Crystallographic date reported in this paper has been deposited with the Cambridge Crystallographic Date Center and allocated the deposition numbers CCDC 890201(1), 890203(2), 890205(L_2), 890206(L_1). Copies of these information may be obtained free of charge from the Director, CCDC, 12 Union Road, Cambridge CB2 1EZ, UK (fax: +44-1223/336-033; e-mail: deposit@ccdc.cam.ac.uk). Synthetic procedures and detailed experimental information; X-ray crystallographic data (CIF); computation studies; optical measurements; two-photon excited fluorescence (2PEF) spectroscopy and two-photon absorption (2PA) cross-section; cell image; microscopy; cytotoxicity assays in cells; These information are available free of charge via the Internet at http://pubs.acs.org.

References

(1) Y. Q. Tian, C. Y. Chen, C. C.Yang, A. C. Young, S. H. Jang, W. C. Chen, and A. K. Y. Jen, *Chem. Mater.* **2008,** 20, 1977-1987.

(2) L. Donato, A. Mourot, C. M. Davenport, *Angew. Chem. Int. Ed.* **2012**, 51, 1840-1843.

(3) W.Huang, F. S. Tang, B. Li, J. H. Su And H. Tian, *J. Mater. Chem. C.* **2014**, 2, 1141-1148.

(4) F. Charra and M. P. Teulade-Fichou. *J. Am. Chem. Soc*. **2013**, 135, 12697-12706.

(5) G. Garcia, F. Hammerer, F. Poyer, S. Achelle, M. P. Teulacle-Fichou, P. Maillard, *Bioorg. Med. Chem.* **2013**, 21, 153-165.

(6) L. Li, C. W.Zhang, G. Y. J. Chen, B. W. Zhu, C. Chai, Q. H. Xu, E. K.Tan, Q. Zhu, K. L. Lim and Q. Y. Shao. *Nat. Commun.*, **2014**, 5, 3276-3285.

(7) J. L. Geng, C. C. Coh, N. Tomczak, J. Liu, R. R. Liu, L. Ma, L. G. Ng, G. G. Gurzadyan And B. Liu. *Chem. Mater.* **2014**, 26, 1874-1880.

(8) M. C. Cui, M. Ono, H. Watanabe, H. Kimura, B. Liu and H.Saji. *J. Am. Chem. Soc.* **2014**, 136, 3388-3394.

(9) K.Rathore, C. S. Lim, Y. Lee and B. R. Cho. *Org. Biomol. Chem.* **2014**, 12, 3406-3412.

(10) Y. Hu , C. H. Heo, G. Kim, E. J. Jun, J. Yin, H. M. Kim And J. Yoon , *Anal. Chem*. **2015**, 87, 3308-3313.

(11) M. Li, S. Yang, Z. Y. Peng, C. H. Liu, J. S. Li, W. W. Zhong, R. H. Yang, And W. H. Tan, *Anal. Chem.* **2014**, 86, 3548-3554.

(12) W. C. Xu, J. R. Zuo, L. L. Wang, L. N. Ji and H. Chao, *Chem. Commun*., **2014**, 50, 2123-2125.

(13) L.Yuan, L. Wang, B. K. Agrawalla, S.-J.Park, H. Zhu, B.-Sivaraman, J. J. Peng, Q.-H. Xu and Y. -T. Chang, *J. Am. Chem. Soc.,* **2015**, 137(8), 5930-5938.

(14) A. S.Dvornikov, E. P. Walker and P. M. Rentzepis. *J. Phys. Chem. A*, **2009**, 113, 13633-13644.

(15) Z. Q.Li, N. Pucher, K. Cicha, J. Torgensen. S. C. Ligon, A. Ajami, W. Husinsky, A. Rosspeintner, E. Vauthey, S. Naumov, T. Scherzer, J. Stampfl and R. Liska. *Macromolecules*. **2013**, 46, 352-361.

(16) G. Chen, T. Y. Ohulchanskyy, R. Kumar, H. Ågren and P. N. Prasad, *ACS Nano*. **2010**. 4(6). 3163-3168.

(17) H. P. Wu, H. W. Yu, Z. H. Yang, X. L. Hou, X. Su, S. L. Pan, K. R. Poeppelmeier And J. M. Rondinelli. *J. Am. Chem. Soc.*, **2013**, 135, 4215-4218.

(18) H. M. Kim and B. R. Cho, *Chem. Rev.* **DOI:10.1021/cr5004425.**

(19) Y. H. Jiang, Y. C.Wang, J. L. Hua, J. Tang, B. Li, S. X. Qian and H. Tian. *Chem. Commun.* **2010**, 46, 4689–4691.

(20) S. J. Chung, M. Rumi, V. Alain, S. Barlow, J. W. Perry and S. R. Marder. *J. Am. Chem. Soc.* **2005**, 127, 10844-10845.

(21) J. J. Shao, Z. P. Guan, Y. L. Yan, C. J. Jiao, Q. H. Xu and C.Y. Chi. *J. Org. Chem.* **2011**, 76, 780–790.

(22) G. G. Dubinina, R. S. Price, K. A. Abboud, G. Wicks, P. Wnuk, Y. Stepanenko, M. Drobizhev, A. Rebane and K. Schanze, *J. Am. Chem. Soc.* **2012,** 134, 19346-19349.

(23) B. K. Agrawalla, Y. Chandran, W. -H. Phue, S. -C. Lee, Y. -M. Jeong, S. Y. Diana, N. -Y. Kang and Y. -T. Chang, *J. Am. Chem. Soc.* **2015**, 137, 5355-5362.

(24) C. D. Geddes, J. R. Lakowicz, (Eds.), Topics in Fluorescence sensing, Vol. 10, Speinger-Verlag, New York, 2005.

(25) Z. Huang, R. Wang, D. Jia, M. Y.Li, M. G.Humphrey and C. Zhang, *Appl. Mater. Interfaces*. **2012**, 4, 1553-1559.

(26) L. Li, X. Q. Shen, Q. -H. Xu and S. Q. Yao, *Angew. Chem. Int. Ed.* **2013**, 52, 424-428.

(27) M. Pawlicki, H. A. Collins, R. G. Denning and H. L. Anderson, *Angew.*

Chem. Int. Ed. **2009**, 48, 3244-3266.

(28) T. Schwich, M. P. Cifuentes, P. A. Gugger, M. Samoc and M. G. Humphrey. *Adv. Mater.*, **2011**, 23, 1433-1435

(29) Y. P. Fan, J. Y. Zhao, Q. F. Yan, P. R. Chen and D. H. Zhao. *ACS. Appl. Mater. Interfaces.*, **2014**, 6(5), 3122-3131.

(30) E. Baggaley, M. R. Gill, N. H. Green, D. Turton, I. V. Sazanovich, S. W. Botchway, C. Smythe, J. W. Haycock, J. A. Weinstein And J. A. Thomas, *Angew. Chem. Int. Ed.*, **2014**,53, 3367-3371.

(31) E. Baggaley, S. W. Botchway, J. W. Haycock, H. Morris, L. V. Sazanovich, J. A. G. Williams and J. A. Weinstein, *Chem. Sci*., **2014**, 5, 879-886.

(32) P. Y. Zhang, L. M. Pei, Y. Chen, W. C.Xu, Q. T. Lin, J. Q.Wang, J. H. Wu, Y. Shen, L. N. Ji, and H. Chao, *Chem. Eur. J*. **2013**, 19, 15494-15503.

(33)H. M. Kim and B. R. Cho. *Chem. Asian J.* **2011**, 6, 58-59.

(34) G. S. He, L. S. Tan, Q. Zheng, P. N. Prasad, *Chem. Rev*. **2008**. 108. 1245-1330.

(35) F. Todescato, I. Fortunati, S. Carlotto, C. Ferrante, L. Grisanti, C. Sissa, A. Painelli, A. Colombo, C. Dragonetti and D. Roberto, *Phys. Chem. Chem. Phys.* **2011**, 13, 11099-11109.

(36) Q. D. Zheng, G. S. He, P. N. Prasad, *J. Mater. Chem.* **2005**, 15, 579-587;

(37) S. J. K. Pond, O. Tsutsumi, M. Rumi, O. Kwon, E. Zojer, J. L. Bredas, S. R. Marder, J. W. Perry. *J. Am. Chem. Soc.* **2004**, 126, 9291-9306.

(38) A. Wild, A. Winter, F. Schlütter, U.S. Schubert, *Chem. Soc.Rev.* **2011**, 40, 1459-1511.

(39) S. Bhowmik, B. N.Ghosh, V. Marjomäki and K. Rissanen. *J. Am. Chem. Soc.*, **2014**, 136, 5543-5546.

(40) T. C.He, Y. Gao, R. Chen, L. Ma. D.Rajwar, Y. Wang, A. C. Grimsdale, and H.D.Sun. *Macromolecules*, **2014**, 47, 1316-1324.

(41)B. G. Zhang, Y. J. Li, R. Liu, T. M. Pritchett, J. E. Haley And W. F. Sun, *Appl. Mater. Interfaces*., **2013**, 5, 565-572.

(42) Z. Chen, K. M. -C. Wong, E. C. -H. Kwok, N. Zhu, Y. Zu and V. W.-W. Yam, *Inorg. Chem*. **2011**, 50, 2125-2132.

(43) A. Fermi, G.Bergamini, M. Roy, M. Gingras and P. Geroni. *J. Am. Chem. Soc.*, **2014**, 136, 6395-6400.

(44) Y. H. Lee, N. V. Nghia, M. J. Go, J. S. Lee,S. U. Lee And M. H. Lee. *Organometallics*, **2014**, 33, 753-762.

(45) N. Rendón, A. Bourdolle, P. L. Baldeck, H. L. Bozec, C. Andraud, S. Brasselet, C. Copéret and O. Maury. *Chem. Mater.* **2011,** 23, 3228-3236.

(46) F. X. Zhou, Z. Zheng, H. P. Zhou, W. Z. Ke, J. Q. Wang, Z. P. Yu, F. Jin, J. X. Yang, J. Y. Wu and Y. P. Tian. *CrystEngComm.* **2012**, 14, 5613-5621.

(47) H. P. Zhou, F. X. Zhou, P. Wu, Z. Zheng, Z. P. Yu, Y. X. Chen, Y. L. Yu, L. Kong, J. Y. Wu, Y. P. Tian, *Dyes and Pigments.* **2011**, 91, 237-247.

(48) N. Y. Hoang, T. Lathion, L. Guenee, E. Terazzi and C. Piguet, *Inorg. Chem.* **2012**, 51, 8567-8575.

(49) X. C.Wang, X. H. Tian, Q.Zhang, P.P.Sun, J. Y. Wu, H. P. Zhou, B. K. Jin, J. X. Yang, S. Y. Zhang, C. K.Wang, X. T. Tao, M.H. Jiang and Y. P. Tian, *Chem. Mater.* **2012**, 24, 954−961.

(50) K.Sénéchal-David, A. Hemeryck, N. Tancrez, L. Toupet, J. A. G.Williams, I. Ledoux, J. Zyss, A. Boucekkine, J.-P. Guégan, H. Le Bozec, O. Maury, *J. Am. Chem. Soc.* **2006**, 128. 12243-12255.

(51) P. Ghosh.and P. K. Bharadwaj. *J. Am. Chem. Soc.* **1996,** 118, 1553-1554.

(52) R. Hao, M. Li, Y.Wang, J. Zhang, Y.Ma, L.Fu, X. F. Wen, Y. S. Wu, X. C.Ai, S. W. Zhang and Y. G. Wei. *Adv. Func. Mater.* **2007**, 17, 3663-3669.

(53) Z. R. Grabowski, K. Rotkiewicz and W. Rettig, *Chem. Rev.* **2003,** 103, 3899-4031.

(54) S. M. Ji, J. Yang, Q. Yang, S. S.Liu, M. D.Chen, J. Z.Zhao, *J. Org. Chem.,* **2009**, 74, 4855-4865.

(55) S. A.Patel, M. Cozzuol, J. M. Hales, C. I. Richards, M. Sartin, J. C. Hsiang, T.Vosch, J. W. Perry, R. M. Dickson, *J. Phys. Chem. C.,* **2009,** 113, 20264-20270.

(56) M. Irie, K. Sayo, *J. Phys. Chem.,* **1992**, 96, 7671-7674

(57) R. M. Edkins, A. Wriglesworth, K. Fucke, S. L. Bettington and A. Beeby. *Dalton Trans.,* **2011,** 40, 9672-9678.

(58) J. E. Rogers, J. E. Slagle, D. M. Krein, A. R. Burke*, Inorg. Chem.* **2007**, 46, 6483-6494.

(59) L. Li, Y. P.Tian, J. X. Yang, P. P. Sun, J. Y. Wu, H. P. Zhou, S. Y. Zhang, B. K. Jin, X. J. Xing, C. K. Wang, M. Li, G. H.Cheng, H. H. Tang, W. H. Huang, X. T. Tao and M. H. Jiang, *Chem. Asian J.* **2009**, **4**, 668–680.

(60) M. Rumi, J. E. Ehrlich, A. A. Heikal, J. W. Perry, *J. Am. Chem. Soc.* **2000**, 122, 9500-9510.

(61) M. Barzoukas, C.Runser, A. Fort and M. Blanchard-Desce, *Chem, Phys. Lett.* **1996**, 257, 531-537.

(62) D. M.Li, Q. Zhang, P. Wang, J. Y.Wu, Y. H. Kan, Y. P. Tian, H. P.Zhou, J. X.Yang, X. T. Tao and M. H. Jiang, *Dalton Trans.* **2011**, 40, 8170–8178.

Table of Contents entry:

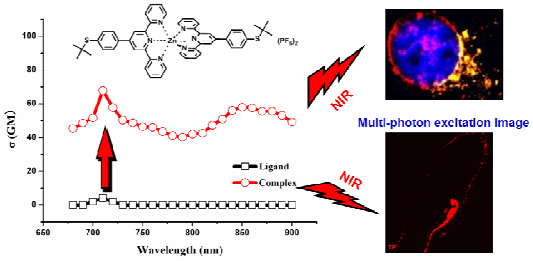

TPA cross sections are enhanced for the complexes containing D-A type ligand $\mathbf{L_1}$. **1** exhibits specificity in two-photon fluorescent imaging.